X_2YZ X = 3d, Y = 5f

X = 8A: Ni
Y = 4A: U
Z = 4B: Sn

Owing to the relative size of the actinide atoms, very few compounds form with 5f elements. At room temperature Ni_2USn has the $L2_1$ structure, but transforms at 220 K to a lower symmetry phase.

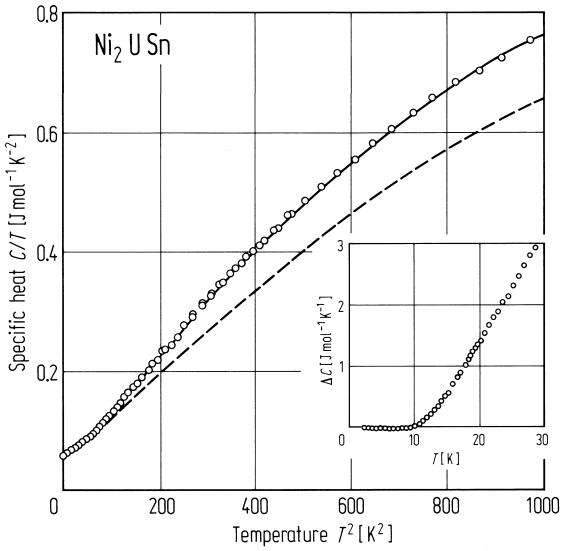

Fig. 361. Specific heat divided by temperature vs. temperature squared for Ni_2USn. The curve is the best overall fit, using electronic plus full Debye contributions. The broken curve is a better two-contribution fit to the low T (< 10 K) data. The inset shows the difference between this fit and the data [90E1].

1.5.5.8 Hyperfine fields

Since the previous review [88W1] a substantial amount of research has been undertaken to determine the hyperfine fields at all three sites. Measurements have also been undertaken as a function of pressure and on systems undergoing phase transitions. Detailed band structure calculations and predictions of hyperfine fields have also been published.

X_2YZ X = 3d, Y = 3d, 4d, 5d,

X = 8A: Co
Y = 4A: Ti, Zr, Hf; 5A: V, Nb; 6A: Cr; 8A: Fe
Z = 3B: Al, Ga; 4B: Si, Ge, Sn

Co_2YZ

The hyperfine field at the Z site has been investigated using ^{119}Sn Mõssbauer effect. Time differential perturbed angular correlating (TDPAC) measurements of Cd hyperfine fields have also been carried out. All the samples are ferromagnetic with the moment confined to the Co sites.

The ^{59}Co and ^{55}Mn NMR have been measured at 4.2 K by the spin echo technique. The measurements at the Y site were carried out by dilute substitution of Mn. The hyperfine field at the Y site was found to be 30-80 kOe higher than that in Co_2 Mn Z alloys with the same Z [89K1].

Table 73. Mössbauer effect and magnetisation results for Co_2YZ alloys [84R1].

Host	p_{Co} [μ_B]	H(Sn) [kOe]	IS [mm s^{-1}]	H(Sn)/p [kOe μ_B^{-1}]
Co_2TiAl	0.35	29 ± 2	1.44 ± 0.03	83
Co_2TiGa	0.4	25 ± 2	1.42 ± 0.01	63
Co_2TiSn	0.87	+ 80		+ 92
Co_2VAl	0.92	– 7 ± 2	1.47 ± 0.02	– 8
Co_2VGa	1.05	– 12 ± 2	1.47 ± 0.02	– 11
Co_2VSn	0.31	+ 7		+ 23
Co_2CrAl	0.80 ± 0.02	49 ± 2	1.40 ± 0.02	61
Co_2CrGa	1.21 ± 0.02	– 61 ± 2	1.41 ± 0.02	– 50

Table 74. Cd and Sn hyperfine fields measured in Co based Heusler alloys Co_2YZ. The values are extrapolated to 0 K and are quoted in kOe [87Y1].

Alloy	H_{hf} (Cd) [kOe]	H_{hf} (Sn) [kOe]
Co_2TiAl	70(6)	29(2)
Co_2TiGa	– 108(6)	25(2)
Co_2TiGe	143(5)	
Co_2TiSn		+ 83
Co_2VAl	– 64(3)	– 7(2)
Co_2VGa	– 56(5)	– 12(2)
Co_2VSn		+ 7
Co_2CrAl		49(2)
Co_2CrGa		– 61(2)
Co_2ZrSn	180(5)	+ 103.5
Co_2NbSn		+ 15
Co_2HfSn		+ 106

Table 75. The Mn hyperfine field $H_{hf}(Mn^{dil}/T)$ in $Co_2(T_{0.95}Mn_{0.05})Z$, the difference ΔH_{hf}(Mn/T) which is defined for the compounds with the same Z by $H_{hf}(Mn^{dil}/T) - H_{hf}(Mn)$ as in Table 77 and magnetic moments [89K1]. Mn^{dil}: dilute substitution of Mn.

Co_2TZ	p_s [μ_B/f.u.]	p_{Co} [μ_B]	H_{hf} (Mn^{dil}/T) [kOe]	ΔH_{hf} (Mn/T) [kOe]
Co_2TiGa	0.75	0.40	– 321 ± 2	– 41
Co_2TiSn	1.93	1.03	– 391 ± 10	– 39 ≈ – 47
Co_2VAl	1.95	0.92	– 357 ± 5	– 76
Co_2VGa	1.92	1.05	– 367 ± 5	– 87
			– 367	
Co_2CrAl	1.55		– 332 ± 5 (weak)	– 52
Co_2CrGa	2.36		– 334 ± 3	– 54
Co_2FeAl	4.96		– 349 ± 5	– 68
Co_2FeGa	5.13		– 332 ± 2	– 52
Co_2FeSi	5.9		– 367 ± 2	– 31

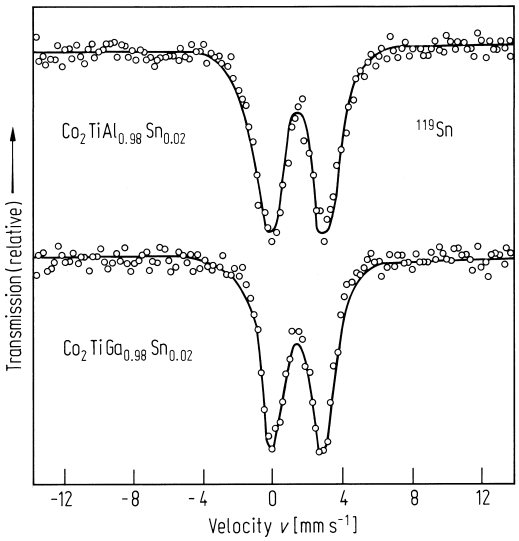

Fig. 362. ^{119}Sn Mössbauer spectra of $Co_2TiAl_{0.98}Sn0_{.02}$ and $Co_2TiGa_{0.98}Sn_{0.02}$ at 4.2 K [84R1].

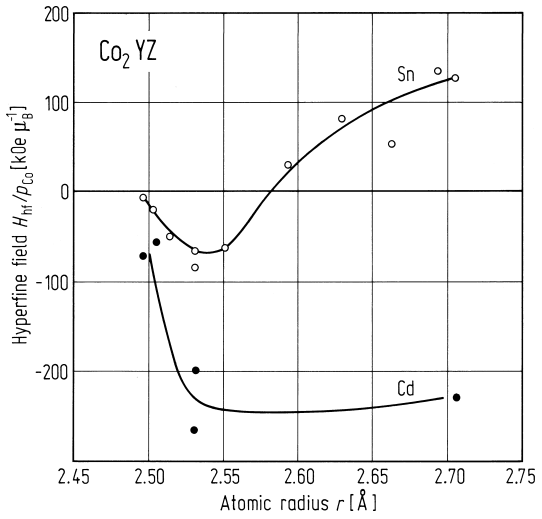

Fig. 364. Reduced hyperfine fields measured at Cd sites (TDPAC) and at Sn sites (Mössbauer) in Co-based Heusler alloys [87Y1].

Fig. 365. Conduction electron polarization in Co-based Heusler alloys calculated using the Campbell Blandin model [75C1] for Cd sites and for Sn sites [87Y1].

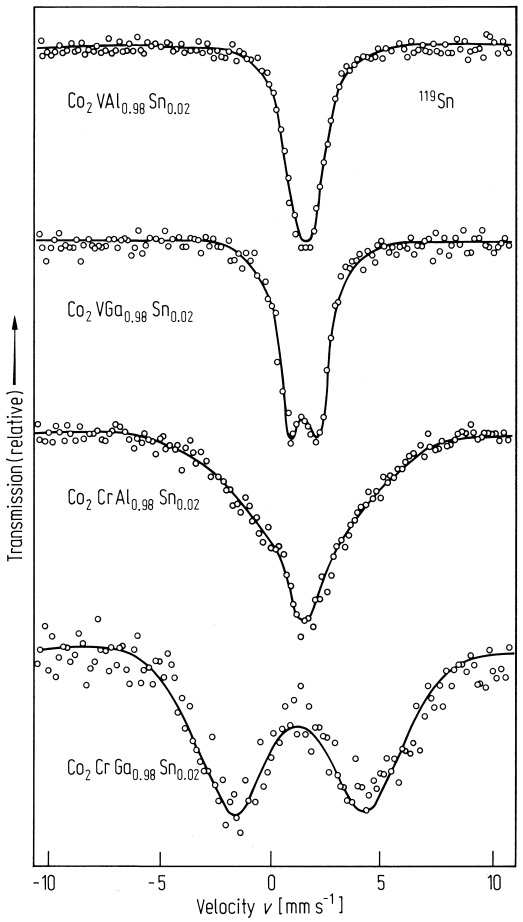

Fig. 363. ^{119}Sn Mössbauer spectra for the Co-based Heusler alloys Co_2VAl, Co_2VGa, Co_2CrAl and Co_2CrGa in which 2 % of Sn has been substituted for either Al or Ga [84R1].

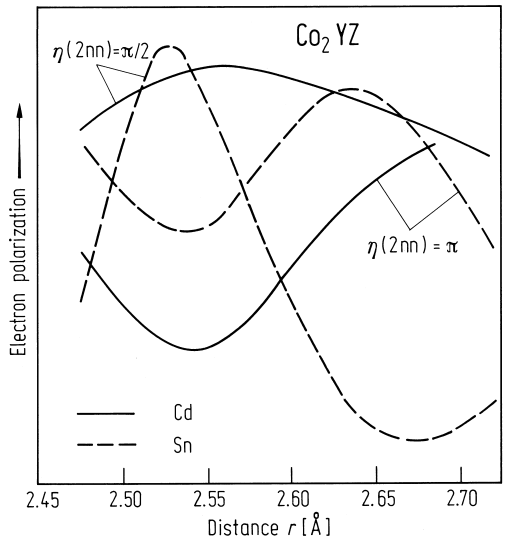

X_2MnZ X = 3d

X = 8A: Co
Z = 3B: Al, Ga; 4B: Si, Ge, Sn; 5B: Sb

Co_2MnZ

All compounds in this series order ferromagnetically with high Curie temperatures. The moment per formula unit is close to 5 μ_B for Z = 4B and approximately 4 μ_B for Z = 3B. The compound containing Sb does not form a single phase system but contains $Co_{1.5}MnSb$ and free cobalt.

Table 76. The Co hyperfine field $(X_{0.95}Co_{0.05})_2MnZ$ which is denoted by $H_{hf}(Co^{dil}/X)$, the difference $\Delta H_{hf}(Co/X)$ which is defined for the compounds with the same Z by $H_{hf}(Co^{dil}/X) - H_{hf}(Co)$ as in Table 77 and magnetic moments [89K1].

X_2MnZ	p_{Mn} [μ_B]	p_{Co} [μ_B]	H_{hf} (Co^{dil}/X) [kOe]	ΔH_{hf} (Co/X) [kOe]
Ni_2MnGa	4.1		– 155 ± 5	17
Ni_2MnSn	3.75	0.75	– 149 ± 3	– 7
Ni_2MnSb	3.71		– 129 ± 3	9
Cu_2MnSn	4.0	0.4	– 144 ± 5	12
Pd_2MnSn	4.21	1.0	– 151	5

Table 77. The Co and Mn hyperfine fields in some Co_2MnZ alloys [89K1].

Co_2MnZ	H_{hf} (Mn) [kOe]	p_{Mn} [μ_B]	H_{hf} (Co) [kOe]	p_{Co} [μ_B]	T_C [K]	a [Å]
Co_2MnAl	280.5	3.01	– 177	0.5	693	5.756
			– 175.1			
Co_2MnGa	280.0	3.01	171.8	0.52	694	5.770
	– 280		– 173			
Co_2MnSi	335.9	3.57	145.0	0.75	985	5.654
	– 337		– 146			
Co_2MnGe	339.4	3.61	140.2	0.75	905	5.743
	– 339		– 141			
Co_2MnSn	344.1	3.58	156.0	0.75	829	6.000
	– 352		– 155			
Co_2MnSb	339	3.76	– 138	0.75	600	5.929

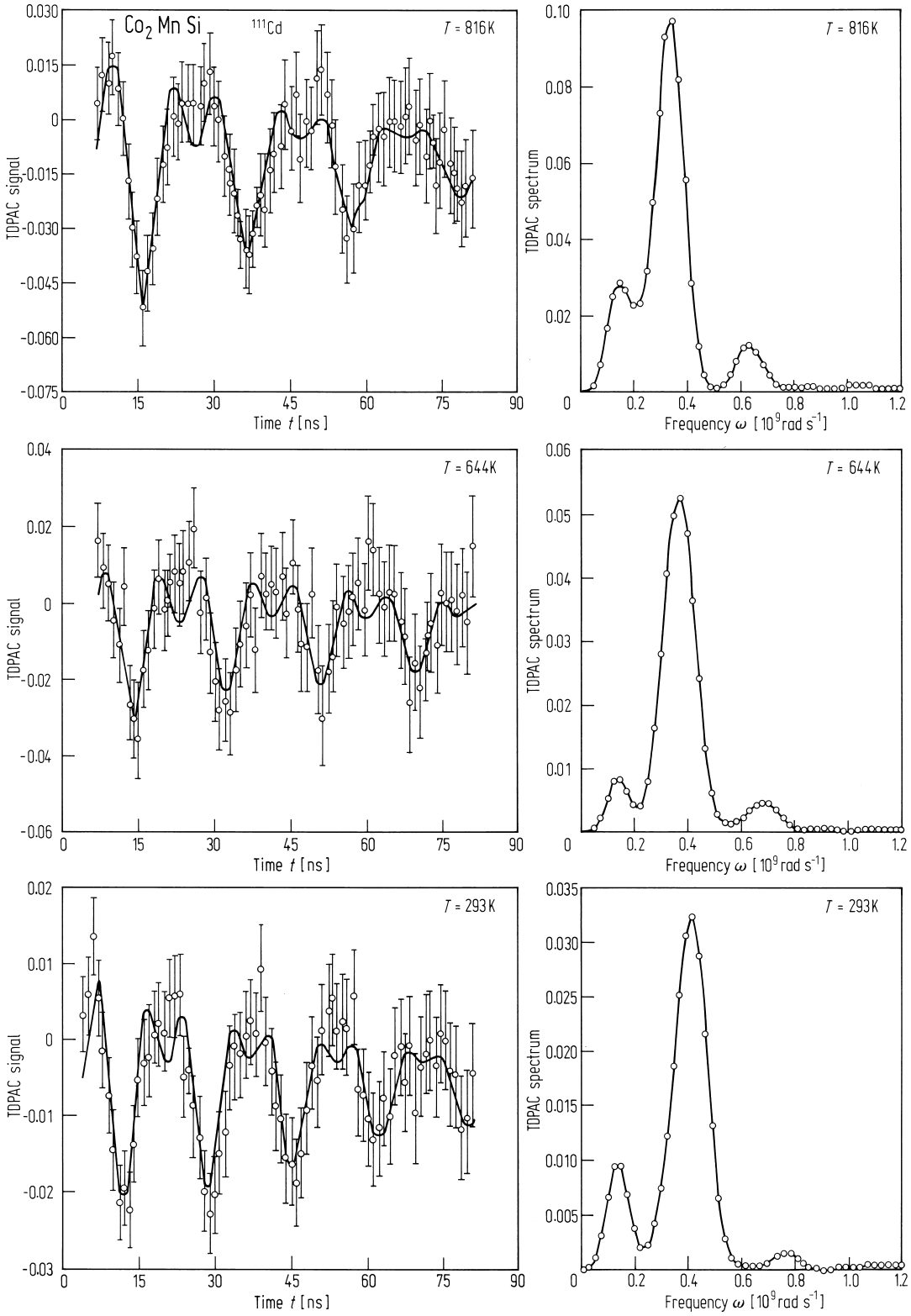

Fig. 366. TDPAC spectra and Fourier transforms for ^{111}Cd in Co_2MnSi at 816 K, 644 K and 293 K [89J1].

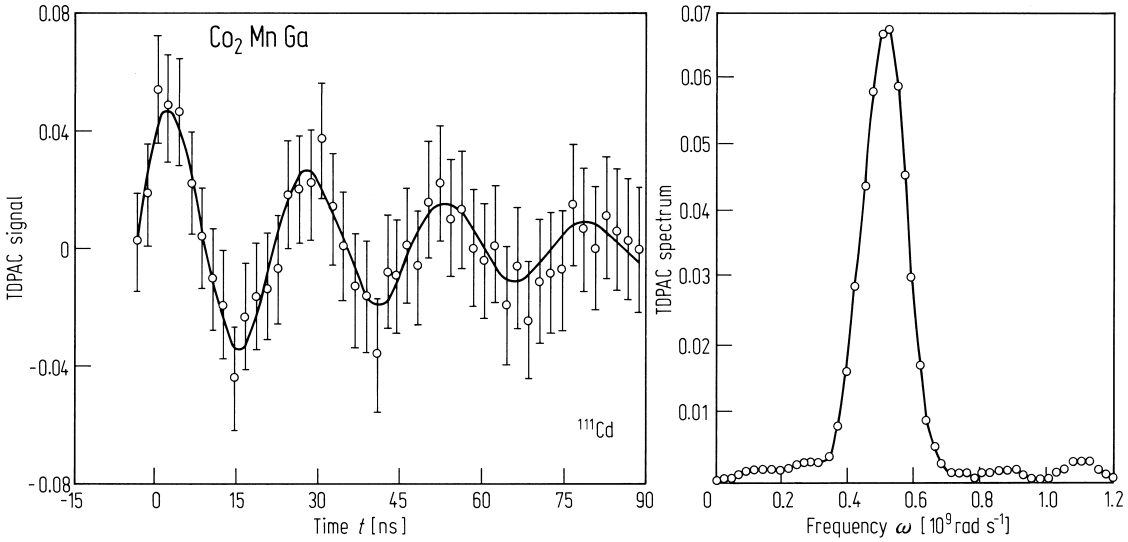

Fig. 367. Room temperature TDPAC spectrum and its Fourier transform for ^{111}Cd in Co_2MnGa with an external polarising field applied [89J1].

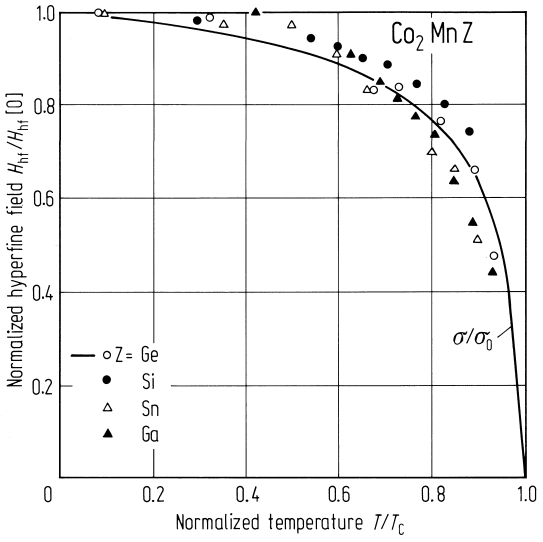

Fig. 368. Hyperfine field at ^{111}Cd sites vs. temperature for Co_2MnZ alloys. The solid line represents the thermal variation of the magnetisation of Co_2MnGe [89J1].

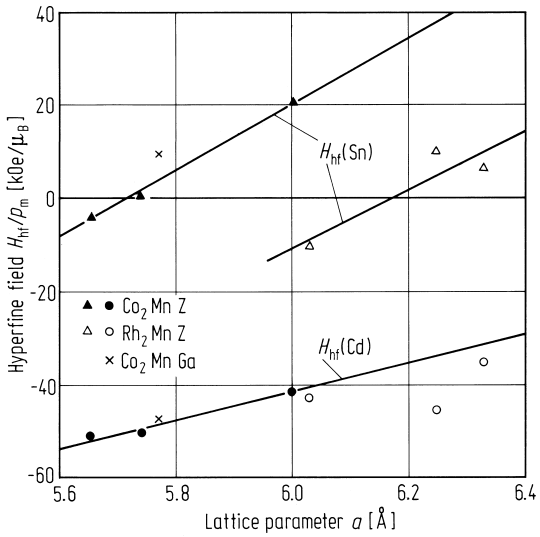

Fig. 369. Hyperfine field normalised to the total magnetic moment per formula unit vs. lattice parameter. Straight lines are fitted respectively to the Cd and Sn hyperfine field in Co_2MnZ and to the Sn hyperfield in Rh_2MnZ (Z = Si, Ge, Sn) [87J1].

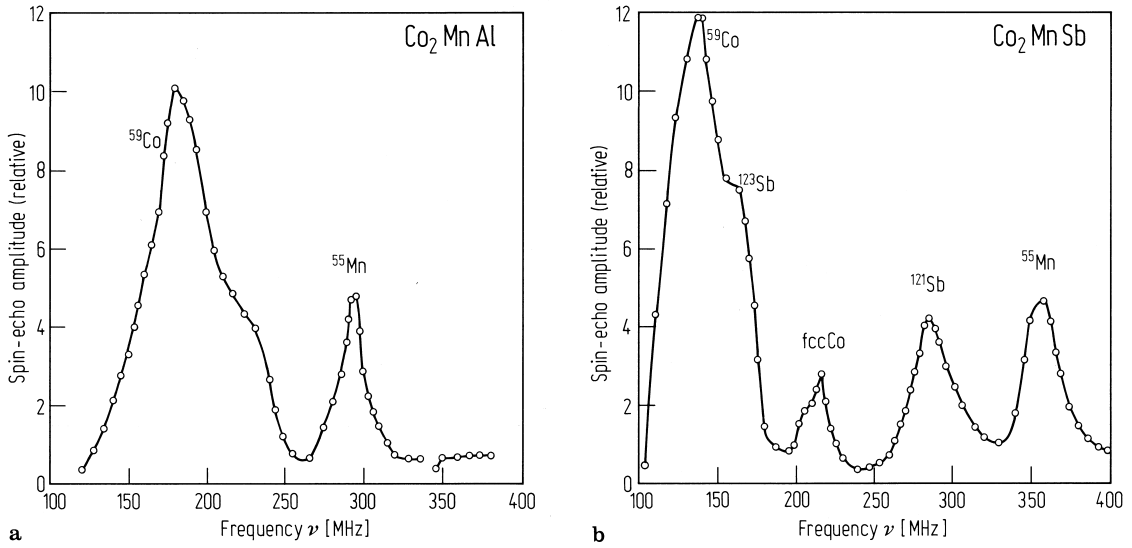

Fig. 370. Zero-field spin-echo amplitude of (**a**) Co_2MnAl and (**b**) Co_2MnSb at 4.2 K [89K1].

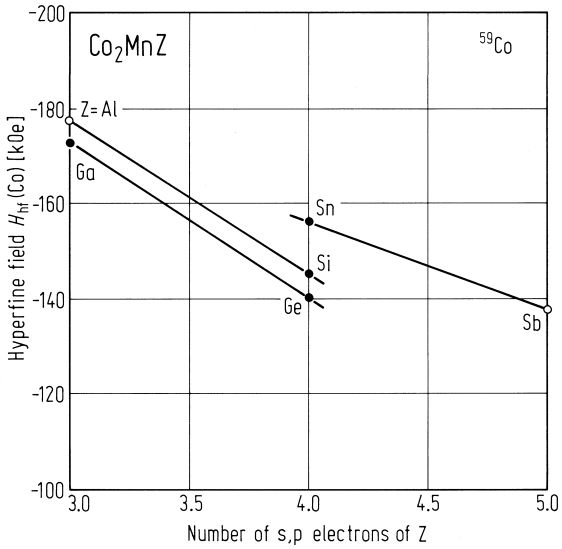

Fig. 371. Co hyperfine field H_{hyp}(Co) in Co_2MnZ as a function of sp electrons on Z [89K1].

Quaternary systems Co_2Mn (Al, Si) and Co_2Mn (Ga, Si)

The effects of changing the conduction electron concentration has been investigated in the alloy system. The results show a linear decrease in the field at the Z site as it changes from a group 3B to a 4B element.

Table 78. Exchange interactions for some cobalt based Heusler alloys [88S1].

Alloy	J_{sf} [MeV]	Alloy	J_{sf} [MeV]
Co_2MnGa	– 59.2	$Co_2MnGa_{0.36}Si_{0.64}$	– 45.9
$Co_2MnGa_{0.77}Si_{0.23}$	– 47.4	$Co_2MnGa_{0.16}Si_{0.84}$	– 36.9
$Co_2MnGa_{0.6}Si_{0.4}$	– 39.7	Co_2MnSi	– 30.6

Table 79. A summary of structural and hyperfine field parameters for compounds in the series $Co_2MnAl_{0.98-x}Si_xSn_{0.2}$ tabulated as a function of x [83D2]. Lattice parameter *a*, Sn hyperfine field *H*, Mössbauer linewidth (HWHM) *Γ*, isomer shift *IS* and Fermi vector k_F.

x	*a* [Å]	*H* [kOe]	*Γ* [mm s^{-1}]	*IS* [mm s^{-1}]	k_F [$Å^{-1}$]
0.00	5.758 ± 0.003	40 ± 1	1.40 ± 0.05	1.51 ± 0.04	1.38
0.20	5.731 ± 0.003	19 ± 1	1.15 ± 0.05	1.44 ± 0.04	1.43
0.40	5.707 ± 0.003	8 ± 1	0.85 ± 0.05	1.45 ± 0.03	1.47
0.58	5.692 ± 0.003	– 7 ± 1	0.80 ± 0.05	1.44 ± 0.02	1.52
0.78	5.674 ± 0.003	– 11 ± 1	0.75 ± 0.05	1.44 ± 0.03	1.56
0.98	5.658 ± 0.003	– 16 ± 1	0.55 ± 0.05	1.45 ± 0.04	1.60

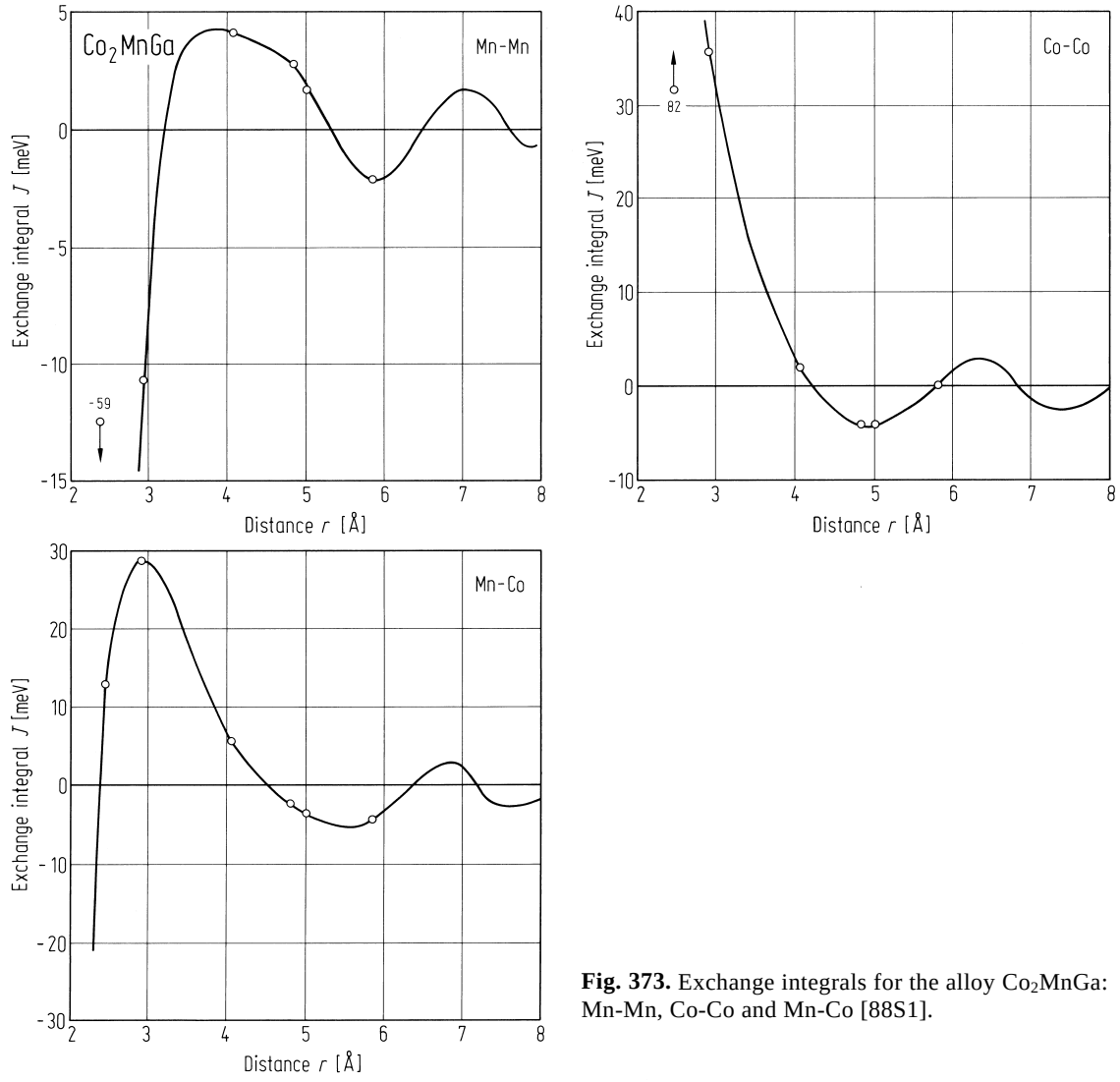

Fig. 373. Exchange integrals for the alloy Co_2MnGa: Mn-Mn, Co-Co and Mn-Co [88S1].

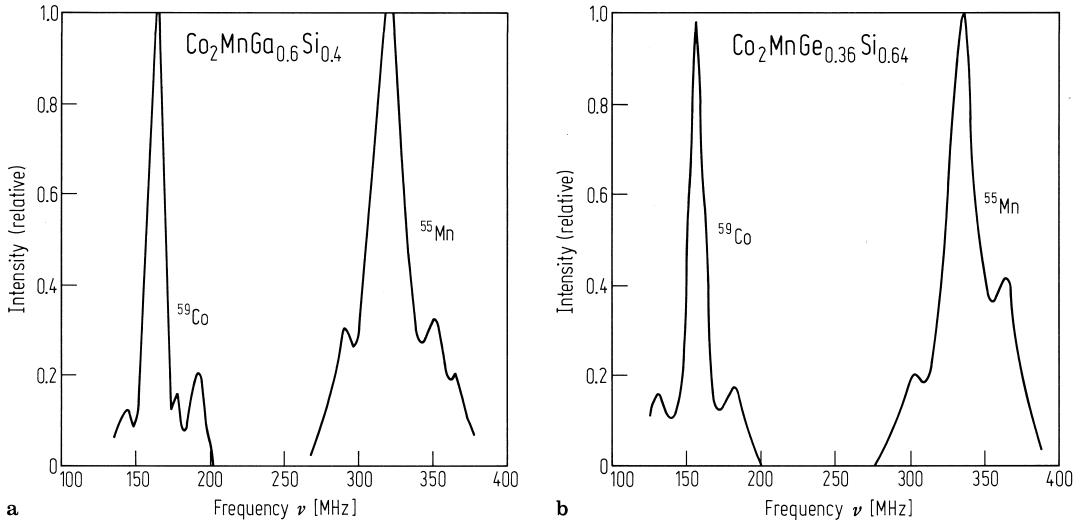

Fig. 372. Spin-echo spectra at 4.2 K in (**a**) $Co_2MnGa_{0.6}Si_{0.4}$ and (**b**) $Co_2MnGe_{0.36}Si_{0.64}$ [88S1].

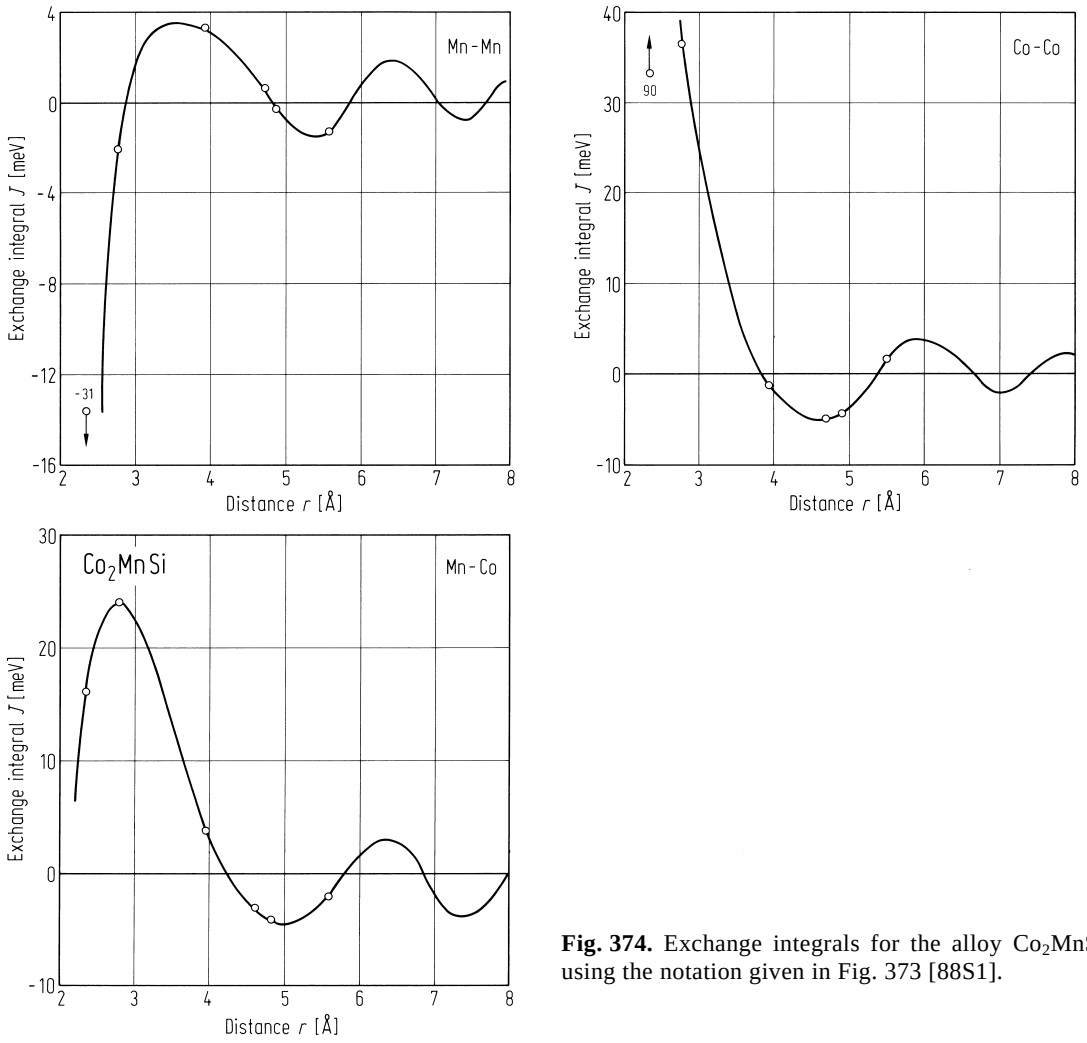

Fig. 374. Exchange integrals for the alloy Co_2MnSi using the notation given in Fig. 373 [88S1].

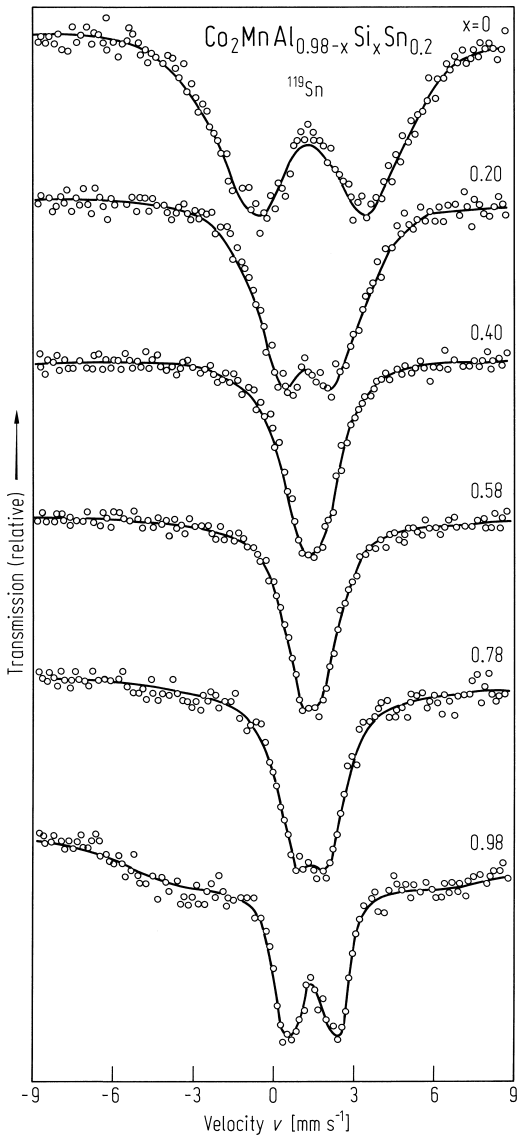

Fig. 375. ^{119}Sn Mössbauer spectra at 77 K of $Co_2MnAl_{0.98-x}Si_xSn_{0.02}$ alloys. The solid lines represent a least squares fit to the data [83D2].

Pressure effects

Table 80. The resonance frequency at 4.2 K, $\nu_{4.2K}$, the corresponding hyperfine field H_{hf}, the pressure dependence of the resonance frequency $(1/\nu)(\partial\nu/\partial p)$ for ^{55}Mn and ^{59}Co and Curie temperature in Co_2MnZ alloys [87K2].

(**a**) ^{55}Mn resonance.

Co_2MnZ	T_C [K]	$\nu_{4.2K}$ [MHz]	H_{hf} [kOe]	$(1/\nu)(\partial\nu/\partial p)$ [10^{-3} GPa^{-1}]
Co_2MnSi	985	354.5 ± 0.3	– 335.9	– 1.61 ± 0.04
Co_2MnGe	905	358.2 ± 0.3	– 339.4	– 1.20 ± 0.06
Co_2MnSn	829	363.1 ± 0.3	– 344.1	– 1.19 ± 0.03
Co_2MnGa	694	295.5 ± 0.4	– 280.0	+ 1.86 ± 0.03

(**b**) ^{59}Co resonance.

Co_2MnZ	T_C [K]	$\nu_{4.2K}$ [MHz]	H_{hf} [kOe]	$(l/\nu)(\partial\nu/\partial p)$ [10^{-3} GPa^{-1}]
Co_2MnSi	985	146.5 ± 0.2	– 145.0	– 4.26 ± 0.14
Co_2MnGe	905	141.6 ± 0.2	– 140.2	– 3.94 ± 0.07
Co_2MnSn	829	157.6 ± 0.3	– 156.0	– 1.82 ± 0.07
Co_2MnGa	694	173.6 ± 0.4	– 171.8	+ 0.52 ± 0.06

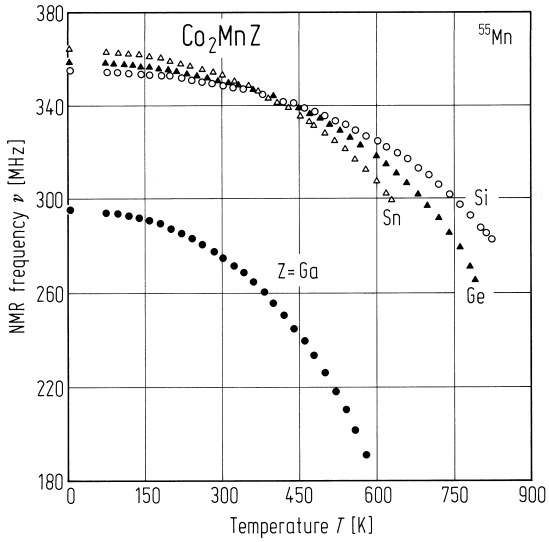

Fig. 376. ^{55}Mn NMR frequency υ vs. temperature in Co_2MnZ alloys were Z = Si, Ge, Sn, Ga [87K2].

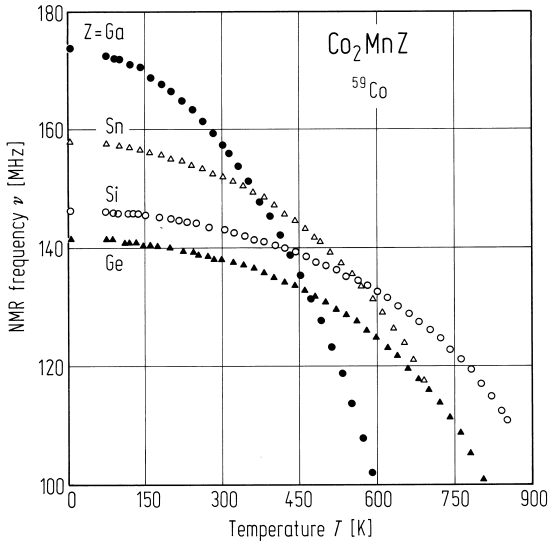

Fig. 377. ^{59}Co NMR frequency υ as a function of temperature T in Co_2MnZ alloys with Z = Si, Ge, Sn, Ga [87K2].

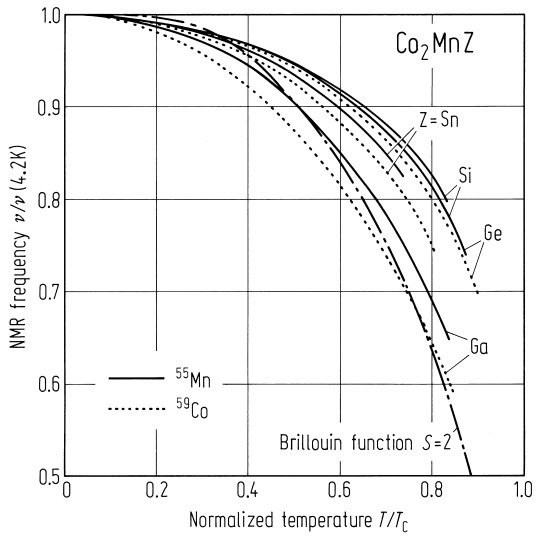

Fig. 378. Normalised frequency $\upsilon/\upsilon_{4.2K}$ vs. reduced temperature T/T_C for Co_2MnZ alloys (Z = Si, Ge, Sn, Ga). The solid lines are for ^{55}Mn and the dotted lines are for ^{59}Co. The ^{59}Co line for Z = Si and the ^{55}Mn line for Z = Ge almost overlap. The broken curve represents the variation of a Brillouin function for S = 2 [87K2].

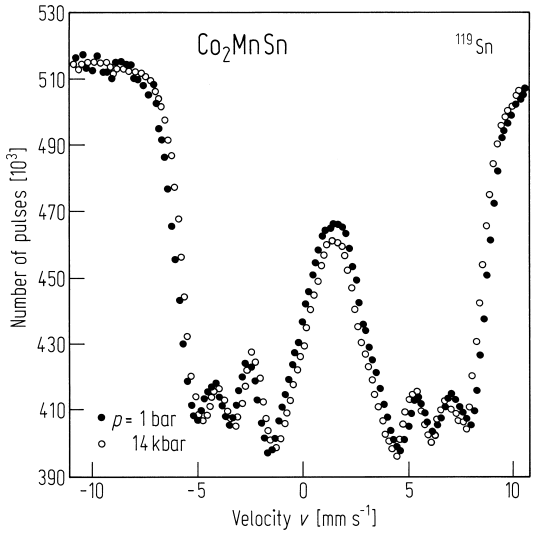

Fig. 379. Mössbauer spectra of the ^{119}Sn nuclei in Co_2MnSn for two different applied pressures of 1 bar and 14 kbar [75N1].

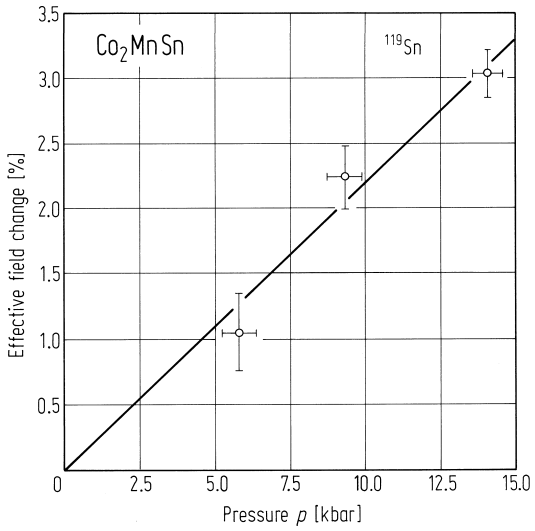

Fig. 380. Relative change in the effective field at the ^{119}Sn nuclei in Co_2MnSn as a function of applied pressure [75N1].

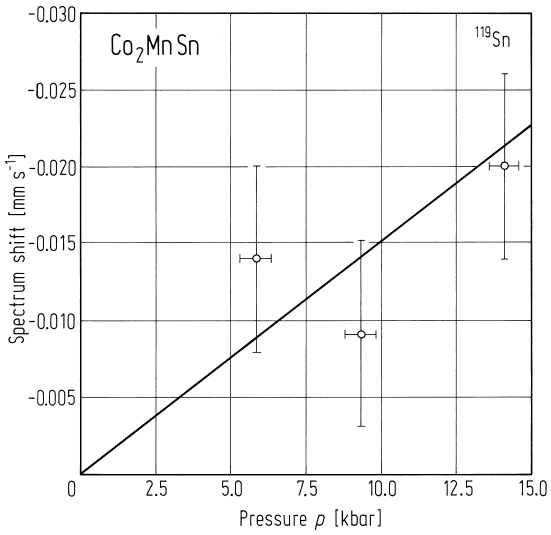

Fig. 381. Change in the position of the centre of gravity of the spectrum of the ^{119}Sn nuclei in Co_2MnSn as a function of applied pressure [75N1].

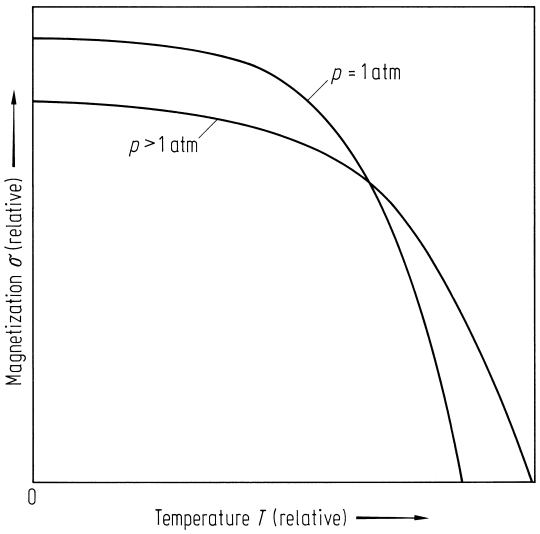

Fig. 382. Schematic temperature variation of the magnetisation for (*1*) p = 1 atm and (*2*) p > 1 atm [75N1].

X_2YZ X = 3d, Y = 3d

X = 7A: Mn

Y = 8A: Co, Ni

Z = 4B: Sn

Mn_2YSn

The compounds which are ferromagnetic are of particular interest since the Mn atoms occupy the tetrahedral sites.

Table 81. A summary of the structural and magnetic properties of several Heusler alloys [90S3].

Alloy	t_a [h]	T_a [°C]	a [Å]	p_{00} [μ_B]	T [K]
Mn_2CoSn	170	800	6.056 + 0.005	2.66 + 0.05	580 + 5
Mn_2NiSn	170	800	6.096 + 0.005	2.02 + 0.05	533 + 5
Ni_2MnSn	170	850	6.054 + 0.005	4.02 + 0.05	353 + 5
Co_2MnSn	24	720	6.00	5.08 + 0.05	329 + 4

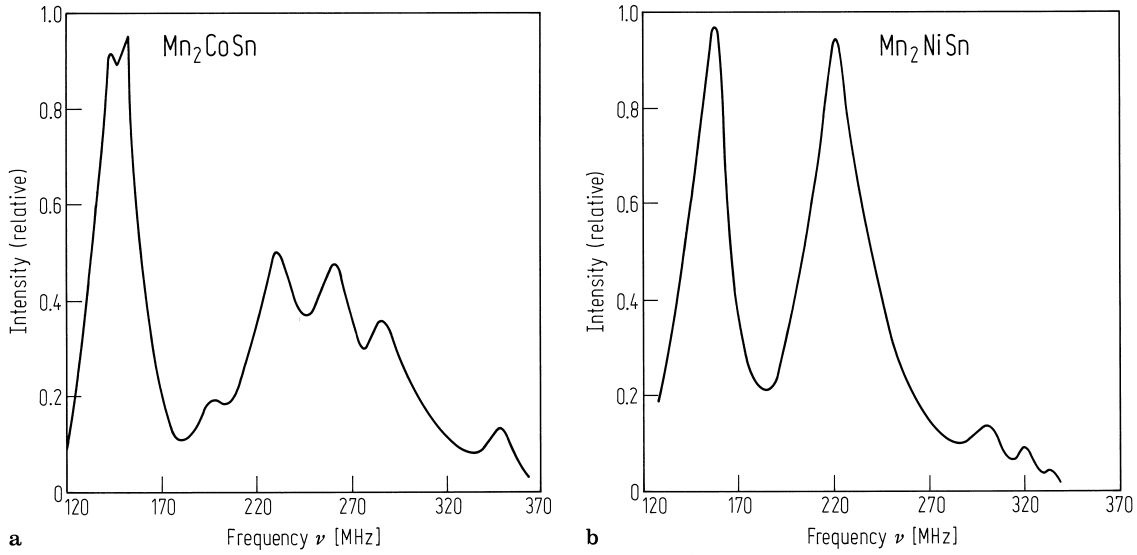

Fig. 383. Nuclear spin echo spectra of the Heusler alloys (**a**) Mn_2CoSn and (**b**) Mn_2NiSn at T = 1.4 K in zero external field [90S3].

X_2YZ X = 3d, Y = 3d, Z = 4B

X = 8A: Fe

Y = 7A: Mn

Z = 4B: Si

Fe_2Mn Si

The compound orders ferromagnetically below 214 K but undergoes a phase transition to a canted structure at 69 K. The effects of the atomic environment on the magnetic properties has been investigated using the hyperfine field on ^{57}Fe.

Table 82. $N(n)$ is the relative number of iron atoms on the B and D sites with n nearest neighbour iron atoms. x is the concentration of iron atoms on the C sites. *IP* is the relative integrated intensity under each peak in the $P(H)$. H_i is the magnetic hyperfine field at each peak in the $P(H)$ [91G1].

Fe_2MnSi (x = 0.1)				$Fe_{1.5}Mn_{1.5}Si$ (x = 0.01)			
n	*N*(*n*) [%]	*IP* [%]	H_i [kOe]	*n*	*N*(*n*) [%]	*IP* [%]	H_i [kOe]
0	62.3	61	64	0	95.4	95	63
1	27.2	29	116	1	3.8	4	115
2	4.6	5	158	2	0.1		
c site	5.0	5	287	*c* site	0.7		

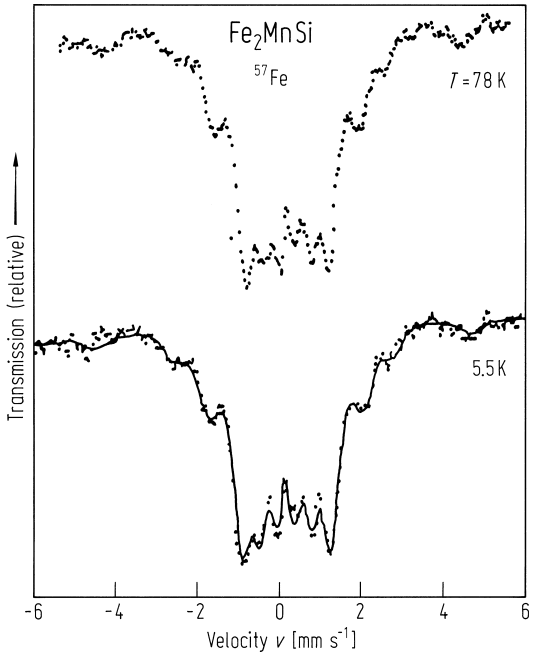

Fig. 384. ^{57}Fe Mössbauer spectra of Fe_2MnSi at 78 and 5.5 K. The solid curve is a theoretical simulation [91G1].

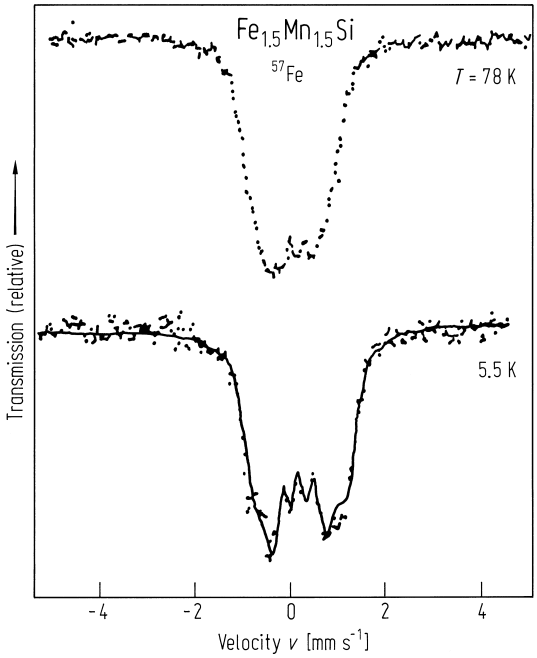

Fig. 385. ^{57}Fe Mössbauer spectra of $Fe_{1.5}Mn_{1.5}Si$ at 78 and 5.5 K. The solid curve is a theoretical simulation [91G1].

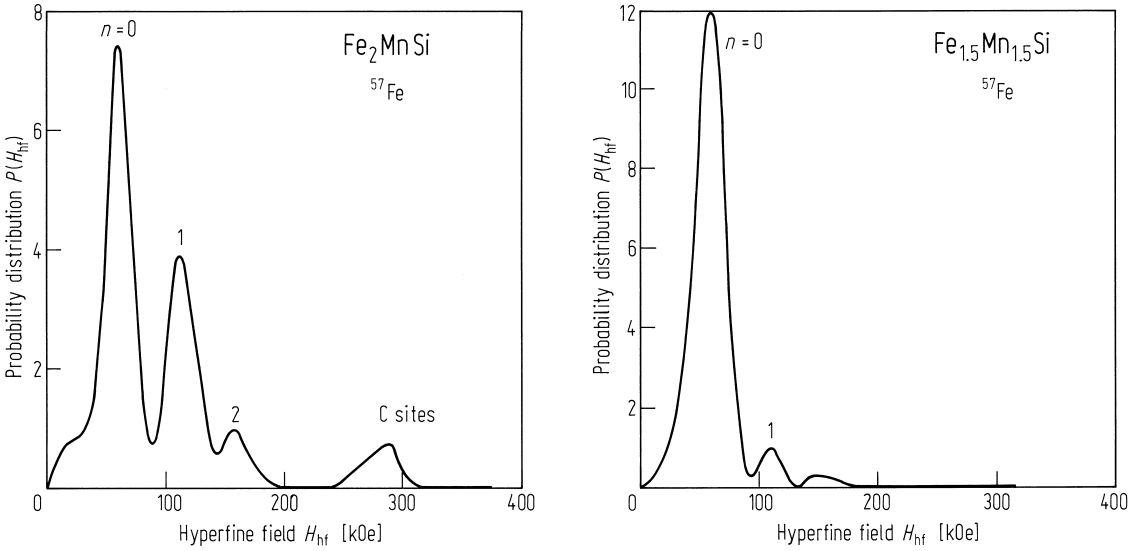

Fig. 386. Distributions of hyperfine field $P(H)$ for the spectra of Fe_2MnSi and $Fe_{1.5}Mn_{1.5}Si$ at 5.5 K. Each peak corresponds to the number n of nearest neighbour iron atoms around an iron atom of the B or D sites (see Figs. 384 and 385) [91G1].

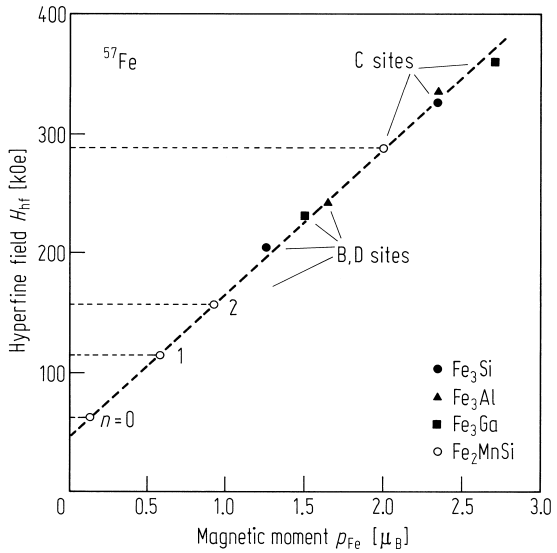

Fig. 387. Relation between ^{57}Fe hyperfine field and magnetic moment of iron atom in several $D0_3$ type alloys. The dotted line indicates the Wertheim relation for p_{Fe} = 1.5 μ_B . For Fe_2MnSi n is the number of nearest neighbour iron atoms around an iron atom on the B or D sites [91G1].

X_2YZ X = 3d, 4d, Y = 3d, Z = 3B

X = 8A: Ni, Pd
Y = 7A: Mn
Z = 3B: Ga; 4B: Sn

Ni_2MnGa

The compound orders ferromagnetically with a moment of approximately 4 μ_B confined to the Mn atom. At approximately 220 K the compound transforms to a tetragonal structure.